*Tellus (2003), 55B, 580–595*
*Printed in UK. All rights reserved*


**TELLUS**
*ISSN 0280–6509*

# TransCom 3 $CO_2$ inversion intercomparison: 2. Sensitivity of annual mean results to data choices

By RACHEL M. LAW[1]*, YU-HAN CHEN[2], KEVIN R. GURNEY[3] and TRANSCOM 3 MODELLERS[4],
[1]*CSIRO Atmospheric Research, PMB 1, Aspendale, Victoria 3195, Australia;* [2]*Department of Earth, Atmospheric, and Planetary Science, Massachusetts Institute of Technology (MIT), Cambridge, Massachusetts, USA;* [3]*Department of Atmospheric Science, Colorado State University, Fort Collins, Colorado, USA;* [4]*D. Baker, P. Bousquet, L. Bruhwiler, P. Ciais, A. S. Denning, S. Fan, I. Fung, M. Gloor, M. Heimann, K. Higuchi, J. John, T. Maki, S. Maksyutov, B. Pak, P. Peylin, M. Prather, P. Rayner, J. Sarmiento, S. Taguchi, T. Takahashi and C-W. Yuen*

(Manuscript received 8 April 2002; in final form 5 December 2002)

ABSTRACT

TransCom 3 is an intercomparison project for $CO_2$ source inversions. Annual mean $CO_2$ concentration data are used to estimate $CO_2$ sources using 16 different atmospheric transport models. Here we test the sensitivity of the inversion to the concentration data. We examine data network choice, time period of data, baseline data selection and the choice of data uncertainty used. We find that in most cases regional source estimates lie within the source uncertainty range of the control inversion. This indicates that the estimated sources are relatively insensitive to the changes in data that were tested. In the data network tests, only the Australian region source estimates varied over a much larger range than that given by the control case uncertainty estimate. For the other regions, the sensitivity to data network was within or close to the uncertainty range. Most of the sensitivity was found to be associated with a small number of sites (e.g. Darwin, Easter Island). These sites are often identified by the inability of the inversion to fit the data at these locations. The model-mean inversion values are mostly insensitive to the time period of data used, with the exception of temperate North America and the tropical Indian ocean. Data selection has a small impact on source estimates for the mean across models, but individual model sensitivity can be large. The magnitude of data uncertainties controls the relative magnitude of the estimated source uncertainty and the spread in model source estimates. Smaller data uncertainties lead to larger differences in source estimates between models. Overall, the data sensitivity tests performed here support the robustness of the control inversion source estimates presented in Gurney et al. (2003. *Tellus* **55B**, this issue). The test results also provide guidance in setting up and interpreting other inversions.

## 1. Introduction

Gurney et al. (2002; 2003) have introduced the TransCom 3 inversion intercomparison project and have presented control annual mean inversion results. Their control case made a number of choices about the atmospheric $CO_2$ dataset that was inverted. They used 1992–1996 (5-yr) mean concentrations at 76 sites from the GLOBALVIEW-$CO_2$ (2000) dataset. These sites were chosen because their records were 70% complete. Data uncertainties were scaled from the residual standard deviations (of individual samples around a smooth curve fit) given in GLOBALVIEW-$CO_2$ (2000) and were modified to set a minimum uncertainty and to account for the uneven spatial distribution of sites. It is important to understand how sensitive the control inversion is to these choices.

*Corresponding author.
e-mail: rachel.law@csiro.au

There is also value in making a more systematic exploration of inversion sensitivity to data choices, since previously only limited tests have been reported. Fan et al. (1998) and Bousquet et al. (1999b) both tested the impact of removing single sites from their data networks and found mostly small impacts. Bousquet (1997) assessed the sensitivity of an inversion to data selection using synchronous sampling time, again showing only a small impact. He also compared sources estimated for two 2-yr periods with his decadal results to explore interannual variability related to El Niño. Significant interannual variability was found. Pacala et al. (2001) also report source estimates for different time periods. Their sensitivity includes impacts due to changing data availability in time, since they gave less weight to sites with little or no data during a given time period. Baker (2001) tested the sensitivity of his inversion results to whether constant or variable (in space) data uncertainties are used. Each of these tests were limited mostly to one or sometimes to two or three transport models. Here we are able to use 16 transport models which submitted data to the TransCom 3 project. A more reliable indication of sensitivity should be obtained using this range of transport models than if one model alone was used.

A number of issues are relevant to testing the data sensitivity of the inversion. The first issue is the choice of observation sites to be used. $CO_2$ concentrations are measured by a number of groups, using either in-situ analysers or by filling flasks for later laboratory analysis. Most of the available $CO_2$ data are brought together in GLOBALVIEW-$CO_2$ (2000; 2001) Those performing inversions have typically made two different choices with regard to data usage. One choice has been to use almost all the available data (regardless of record length or missing data) in order to obtain better spatial coverage. The other choice has been to use only those sites with long (typically greater than 10 yr) records and often from only one measuring program (to avoid any intercalibration differences). Finding a reasonable balance between these two choices of maximising spatial coverage and minimising missing data is a question that warrants more systematic treatment.

The second issue is associated with the time period over which data are used in the inversion. There are large interannual variations in $CO_2$ sources (e.g. Francey et al., 1995; Keeling et al., 1995). For those inversions that do not solve for the whole interannual time history of sources, the atmospheric $CO_2$ concentration data have typically been averaged over a number of years. Various time periods have been used. It would be helpful to know how much of the difference between inversion results has been methodological and how much is contributed by variations in data for the different time periods in the inversion.

The third issue is that of data selection. $CO_2$ observations are usually selected for their 'clean-air' or 'baseline' concentration. In the case of flask measurements, this is determined by filling flasks when the meteorological conditions, e.g. wind direction, imply that the air is representative of a large region. For coastal sites, this means that the air sample is usually from the marine rather than continental direction. In the in-situ case, data are measured at all times but only data collected under baseline conditions are reported in GLOBALVIEW-$CO_2$ (2000). This means that in most inversions, model output for all times is being compared with selected observational data. Both Law (1996) and Ramonet and Monfray (1996) show that selecting model output in a manner similar to the selection of the observations, can have a systematic impact at some sites, e.g. changing the amplitude or phasing of the seasonal cycle. It is important to investigate how these systematic differences between model and observational data impact on the sources estimated by an inversion.

Many inversion methods require an uncertainty to be provided for each observational data record. The uncertainty does not just encompass measurement error, which is typically quite small (0.1–0.2 ppm). It also needs to provide some indication of a model's ability to represent a given site. For example, a model can better represent a remote southern hemisphere site where local sources are small, than a northern hemisphere continental site. This is particularly true for sites that are surrounded by inhomogeneous and relatively unknown sources. Any misrepresentation of the assumed spatial structure of sources in a region will be seen in the inversion as a data error and hence needs to be incorporated into the data uncertainty (Kaminski et al., 2001). Past inversions have set these data uncertainties in different ways, typically using a fixed uncertainty at all sites (e.g. Rayner et al., 1999) or using uncertainties related to the measurement variability at a site (e.g. Bousquet et al., 1999a). Here we compare these cases. We also examine the impact of changing the magnitudes of the data uncertainties.

## 2. Method

There are three components involved in estimating $CO_2$ sources from atmospheric measurements: the inversion method, the transport model and the atmospheric data. Here we keep the inversion method fixed and perform a series of inversions across a range of transport models and data choices.

### 2.1. Inversion

We use a Bayesian synthesis inversion method, solving for 11 land and 11 ocean regions. These regions are shown in Fig. 1 of Gurney et al. (2003), where the inversion method is also described in more detail. We use their inversion as the control inversion here. The inversion returns source estimates for each region and their uncertainties. In most cases, our analysis focuses on the mean results across models. For each region, we calculate the mean and standard deviation of the sources estimated using each model and the mean of the source uncertainties associated with these source estimates. Following Gurney et al. (2002), we refer to the mean uncertainty as the 'within-model' uncertainty and the source standard deviation (a measure of model spread) as the 'between-model' uncertainty.

### 2.2. Models

The inversions are performed with 16 transport models which are described in Table 1 of Gurney et al. (2003). They cover a range of resolutions, advection schemes, subgrid-scale parameterizations and forcing winds. Three models are full general circulation models (GCMs), so that transport occurs 'online' while the others are all 'offline' calculations. Among the offline models, some use GCM winds and others use analysed winds.

### 2.3. Data

The atmospheric data used in these inversions are taken from GLOBALVIEW-$CO_2$ (2000) (or GLOBALVIEW-$CO_2$, 2001 for 1997 data). GLOBALVIEW contains data that have been processed using curve-fitting to provide continuous, synchronous baseline records at all sites from 1979. Missing data are estimated using a data filling technique (Masarie and Tans, 1995). The GLOBALVIEW data processing ensures comparable records whether measurements were originally made in-situ or by filling flasks. GLOBALVIEW also provides residual standard deviations, a product of the curve fitting and an indication of observational variability at a given site. In GLOBALVIEW, no corrections have been made to the data to account for intercalibration differences between measurement programs or between in-situ and flask data.

*2.3.1. Choice of sites.* The control inversion in Gurney et al. (2003) used 1992–1996 mean data from sites which had data records that were at least 70% complete during this period. This was a total of 76 data records at 64 locations. (More than one measurement program has data at some sites). Here we compare this control inversion with cases in which the criteria on the completeness of the record is varied from 30 to 100%. We also compare networks containing sites from all measuring programs (denoted 'ALL') with cases where the sites are restricted to National Oceanic and Atmospheric Administration, Climate Monitoring and Diagnostics Laboratory flasks only (denoted 'NOAA') or to NOAA/CMDL and Commonwealth Scientific and Industrial Research Organization flask programs only (denoted 'NOAA+CSIRO'). NOAA/CMDL runs the largest $CO_2$ monitoring program while CSIRO runs the second largest network and also has an extensive flask comparison project with NOAA/CMDL (Masarie et al., 2001). The eight missing data criteria and three network options provide 24 different sets of sites that we test. The number of data records for each case, which ranges from 20 to 109 records, is given in Table 1, and site locations are shown in Fig. 1. The table also indicates when each site first meets the missing data and measuring program criteria and is consequently introduced to the dataset.

*2.3.2. Time period of data.* We compare the control (1992–1996 mean) inversion with three inversions using 3-yr mean data from 1989–1991, 1992–1994 and 1995–1997. (1997 data were the most recent data available to us at the time the experiments were performed; otherwise it would have been interesting to include the more recent period encompassing an El Niño event in our tests.) We use the same 76 sites with the same uncertainties as in the control. A consequence of using the same sites is that some sites no longer satisfy the 70% data coverage that was required for the control inversion. For example, several of the 76 sites are inactive during 1989–1991. GLOBALVIEW extrapolated values were thus used more extensively for certain sites. However, using the same 76 control sites rather than following the 70% data criteria allows us to focus on inversion changes from the data-averaging

Table 1. *Sites used for each record-completeness criterion and measuring-program case*

| Name | Code | Network | Name | Code | Network | Name | Code | Network | Name | Code | Network |
|---|---|---|---|---|---|---|---|---|---|---|---|
| **100% 20 21 29** | | | **90% 25 32 43** | | | **70% 44 59 76** | | | **50% 60 77 97** | | |
| Alert | alt_00D0 | NOAA | Bermuda W | bmw_00D0 | NOAA | Baltic | bal_00D0 | NOAA | Christmas I | chr_00D0 | NOAA |
| Ascension | asc_00D0 | NOAA | ITN tower | itn496_00C3 | NOAA | CO air 3000m | car030_00D2 | NOAA | Easter I | eic_00D0 | NOAA |
| Bermuda E | bme_00D0 | NOAA | Key Biscayne | key_00D0 | NOAA | CO air 4000m | car040_00D2 | NOAA | Pacific 35S | pocs35_00D1 | NOAA |
| Barrow | brw_00D0 | NOAA | Ragged Pt | rpb_00D0 | NOAA | CO air 5000m | car050_00D2 | NOAA | Pacific 20S | pocs20_00D1 | NOAA |
| Cold Bay | cba_00D0 | NOAA | Seychelles | sey_00D0 | NOAA | Cape Meares | cmo_00D0 | NOAA | Sth China Sea 3N | scsn03_00D1 | NOAA |
| Cape Grim | cgo_00D0 | NOAA | Shemya | shm_00D0 | NOAA | Hungary | hun_00D0 | NOAA | Sth China Sea 6N | scsn06_00D1 | NOAA |
| Crozet | crz_00D0 | NOAA | Alert | alt_02D0 | CSIRO | Iceland | ice_00D0 | NOAA | Sth China Sea 9N | scsn09_00D1 | NOAA |
| Guam | gmi_00D0 | NOAA | Cape Ferguson | cfa_02D0 | CSIRO | Pacific 15S | pocs15_00D1 | NOAA | Sth China Sea 12N | scsn12_00D1 | NOAA |
| Izana | izo_00D0 | NOAA | Cape Grim | cgo_02D0 | CSIRO | Pacific 10S | pocs10_00D1 | NOAA | Sth China Sea 15N | scsn15_00D1 | NOAA |
| Kumakahi | kum_00D0 | NOAA | Mawson | maa_02D0 | CSIRO | Pacific 5S | pocs05_00D1 | NOAA | Mt Waliguan | wlg_00D0 | NOAA |
| Mould Bay | mbc_00D0 | NOAA | Mauna Loa | mlo_02D0 | CSIRO | Pacific 0 | poc000_00D1 | NOAA | Zeppelin | zep_00D0 | NOAA |
| Mace Head | mhd_00D0 | NOAA | South Pole | spo_02D0 | CSIRO | Pacific 20N | pocn20_00D1 | NOAA | Shetland Is | sis_02D0 | CSIRO |
| Midway | mid_00D0 | NOAA | Amsterdam I | ams_11C0 | ALL | Pacific 25N | pocn25_00D1 | NOAA | Jubany | jbn_29C0 | ALL |
| Mauna Loa | mlo_00D0 | NOAA | Schauinsland | sch_23C0 | ALL | Pacific 30N | pocn30_00D1 | NOAA | Zeppelin | zep_31C0 | ALL |
| Palmer Stn | psa_00D0 | NOAA | **80% 29 42 56** | | | Utah | uta_00D0 | NOAA | **40% 65 83 106** | | |
| Samoa | smo_00D0 | NOAA | Halley Bay | hba_00D0 | NOAA | Bass St 6500m | aia065_02D2 | CSIRO | LEF flask | lef_00D0 | NOAA |
| South Pole | spo_00D0 | NOAA | ITN flask | itn_00D0 | NOAA | Cape Rama | cri_02D0 | CSIRO | LEF tower | lef396_00C3 | NOAA |
| Station M | stm_00D0 | NOAA | Pacific 15N | pocn15_00D1 | NOAA | Estevan Pt | esp_06D0 | ALL | Pacific 35N | pocn35_00D1 | NOAA |
| Syowa | syo_00D0 | NOAA | Ulaan Uul | uum_00D0 | NOAA | Minamitorishima | mnm_19C0 | ALL | Pacific 40N | pocn40_00D1 | NOAA |
| Tae-ahn Pen | tap_00D0 | NOAA | Bass St 500m | aia005_02D2 | CSIRO | Plateau Rosa | prs_21C0 | ALL | Sth China Sea 18N | scsn18_00D1 | NOAA |
| Macquarie I | mqa_02D0 | CSIRO | Bass St 1500m | aia015_02D2 | CSIRO | **60% 49 65 83** | | | Sth China Sea 21N | scsn21_00D1 | NOAA |
| Alert | alt_06C0 | ALL | Bass St 2500m | aia025_02D2 | CSIRO | Malta | goz_00D0 | NOAA | Estevan Pt | esp_02D0 | CSIRO |
| Barrow | brw_00C0 | ALL | Bass St 3500m | aia035_02D2 | CSIRO | Pacific 30S | pocs30_00D1 | NOAA | Westerland | wes_23C0 | ALL |
| Mt Cimone | cmn_17C0 | ALL | Bass St 4500m | aia045_02D2 | CSIRO | Pacific 25S | pocs25_00D1 | NOAA | Mt Waliguan | wlg_33C0 | ALL |
| Izana | izo_27C0 | ALL | Darwin | daa_02D0 | CSIRO | Pacific 5N | pocn05_00D1 | NOAA | **30% 68 86 109** | | |
| Mauna Loa | mlo_00C0 | ALL | Alert | alt_06D0 | ALL | Pacific 10N | pocn10_00D1 | NOAA | Azores | azr_00D0 | NOAA |
| Ryori | ryo_19C0 | ALL | Baring Head | bhd_15C0 | ALL | Bass St 5500m | aia055_02D2 | CSIRO | Black Sea | bsc_00D0 | NOAA |
| Samoa | smo_00C0 | ALL | Plateau Rosa | prs_21D0 | ALL | Kosan | ksn_24D0 | ALL | Pacific 45N | pocn45_00D1 | NOAA |
| South Pole | spo_00C0 | ALL | | | | | | | | | |

The sites are listed under the percentage of time between 1992 and 1996 that data are available for that site. The numbers next to each percentage are the number of sites in the 'NOAA' flask only network, the 'NOAA+CSIRO' network and the 'ALL' network at that completeness percentage. The network used by any given inversion contains the sites listed for the relevant criteria and all sites listed for smaller networks that also satisfy the criteria. The site codes are those used in GLOBALVIEW-$CO_2$ (2000). The lowest levels of the itn and lef tower sites have not been used, since these cannot be represented by the relatively low-resolution global transport models used here.

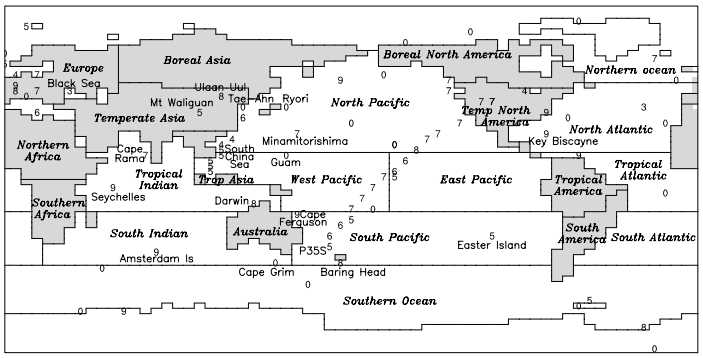


*Fig. 1.* Regions (named in italics) for which sources are estimated by the inversion and sites used (numbers). The region boundaries and site locations are those from the MATCH-MACCM3 model. Other models will use slightly different regions and locations depending on their model grid. The numbers differentiate networks based on the completeness of the data record: 100% complete (0), greater than 90% (9), 80% (8), 70% (7), 60% (6), 50% (5), 40% (4), 30% (3). Where more than one data record exists at a single location, the number indicates the most complete record. Sites that are mentioned in the text are labelled (normal font).

period and to minimise impacts from changing the data network.

In addition to using different data in the inversion, we also change the global growth rate and the fossil-fuel emissions to values representative of the new time periods. At each site, the growth rate has been computed by fitting the $CO_2$ record, over the relevant time period, with a linear trend and two harmonics. We use the mean and standard deviation of the linear trends of the 76 sites to represent the global growth rate, using a conversion factor of 2.123 Gt C ppm$^{-1}$. The global growth rates for the control, 1995–1997, 1992–1994 and 1989–1991 are 3.27, 3.15, 2.37 and 2.76 Gt C yr$^{-1}$, respectively. We use the same growth rate uncertainty of 0.074 Gt C yr$^{-1}$ for all cases. Each model generated two fossil-fuel responses, representing the years 1990 and 1995. For the control inversion, these responses were scaled in the proportions of 20/80% for 1990 and 1995, respectively. For the new inversions, we use proportions for 1995–1997, 1992–1994 and 1989–1991 of 0/100%, 40/60% and 100/0%, respectively.

*2.3.3. Model sampling for baseline data selection.* Two tests are performed in which the model output is sampled in different ways (before averaging for use in the inversion). These tests give a better or worse approximation to baseline-selected observations than the control case. The experimental protocol for TransCom 3 required modellers to submit four-hourly (or similar time frequency) concentrations at a number of specified monitoring locations (Gurney et al., 2000). For most locations, modellers were asked to submit the nearest grid point to the location with a specified surface type (land for continental sites, ocean for coastal and island sites). In some cases where it was known that baseline data are only available from the marine sector, the sampling location in the model was moved further offshore. In the control inversion of Gurney et al. (2003), 20 of the 76 sites used are locations that have been shifted offshore. Therefore baseline selection was partly accounted for in the control inversion. The first test that we perform removes this site-placement accounting of selection by simply using data from the nearest model gridpoint to each site. Coastal sites may be moved onto land depending on each model's grid. This case takes less account of data selection than the control case.

The second test is designed to mimic flask sampling. Since only some of the transport models are run with analysed winds (and even then the output data is only applicable to a single year), we cannot match model output with observations by sampling time. Instead, we assume that flask samples are chosen to avoid air that has recently passed over land, and we approximate this in the model by selecting data using the following procedure. Firstly we use the responses from the land region basis functions to find which land region produces the largest annual mean concentration at the site. We call this the local land region. We assume that flask sampling would avoid air from this region, and so we identify times that the model simulates low concentrations from this local land region source. Hence, the four-hourly concentration timeseries for the local land

region is detrended and divided into 73 five-day segments. In each five-day segment, we identify the third smallest concentration and the time at which it occurs. These times can be thought of as the flask sampling times. We select the third smallest rather than the minimum concentration because some models produce occasional unrealistic low concentrations that are best avoided.

The input to the inversion is the annual mean concentration from each region at each site. For the local land region, we calculate the mean of the 73 selected (low) concentrations. For all the other regions (and the fossil, neutral biosphere and global ocean background fields that are also used in the inversion), the mean is calculated from the concentrations at the same 73 sampling times identified for the local land region. Selection has been applied to all sites, even those that are distant from any land. This avoids applying an arbitrary criterion as to how distant a site should be before selection is no longer appropriate. Thus this 'flask-like' case gives something approaching an upper bound for the impact of selection. One issue that is not addressed in this procedure is how to treat sites that are close to land region boundaries. It is possible that while we have avoided air from the local land region, the selected times could be influenced by air from a neighbouring land region.

*2.3.4. Data uncertainty.* The control inversion of Gurney et al. (2003) used data uncertainties that were based on the variability of the observations at a given site. In generating the data uncertainties that were used, a scaling factor was applied to the GLOBALVIEW residual standard deviations, such that the inversion produced a $\chi^2$ value of approximately one. (See Gurney et al., 2003, for the definition of $\chi^2$). Length of record, proximity to other sites and a minimum uncertainty were also taken into account. Here we compare the control case with inversions where the control data uncertainties are halved and doubled. We also perform an inversion in which a minimum uncertainty (0.25 ppm in the control) was not set and an inversion that uses constant uncertainties of 0.3 ppm for all sites.

## 3. Results

### *3.1. Site choices*

Figure 2 summarises the inversion results using different networks. Mean model sources are shown as differences from the control inversion (Gurney et al., 2003). The mean within-model uncertainty from the control inversion is shown by the box. This indicates whether the spread in estimates from the different networks is large compared to the estimated uncertainty. The three rows of results in each box are the three sets of networks. The '7' in the top row is the control case and hence is always zero. Overall most source estimates lie within the uncertainty range of the control case, which suggests that most regions are not too sensitive to the choice of network. Australia is the most noticeable exception, with estimates lying significantly above and below the uncertainty range. We will examine this region in section 3.1.1.

Other regions also show some notable features. For Europe (whose control flux estimate is $-0.6$ Gt C $yr^{-1}$), using all sites gives estimates that are generally lower (more negative) than when only NOAA/CSIRO sites are used. The ALL case includes sites in Italy and Germany, which have large fossil signatures. Including them in the inversion requires a larger sink to compensate. Boreal Asia shows the opposite result, with the ALL case giving more positive estimates (smaller sinks) than the NOAA/CSIRO networks. It is likely that this region, which has few local sites, is responding to the changes in the European region.

Most networks give estimates that are more positive than the temperate North American control result of $-0.8$ Gt C $yr^{-1}$ , indicating a tendency to smaller rather than larger sinks there. For tropical Asia the three cases give similar estimates for small networks (90 and 100%) and for large networks (30–50%) that include the South China Sea data. For intermediate networks (60–80%) the estimates are more erratic, as the cases are influenced by different more distant sites (e.g. Darwin for the NOAA+CSIRO case, Minamitorishima for the ALL case).

The ocean region with the largest spread of estimates is the South Pacific, mostly due to the gradual introduction of the Pacific ocean ship data. Easter Island (29°S, 109°W) comes into the network at 50% and the estimates drop significantly (by almost 1 Gt C $yr^{-1}$ for the NOAA-only case). The data mismatch at Easter Island is about 1 ppm, suggesting that an even larger uptake would be required to fit this datum alone but a compromise with the higher concentration Pacific ship data is moderating the uptake. One contributor to the data mismatch is that the inversion estimates the ocean sources as differences from the Takahashi air–sea flux distribution (Takahashi et al., 1999). This set of fluxes gives higher concentrations at Easter Island than at the 25°S and 30°S ship locations,

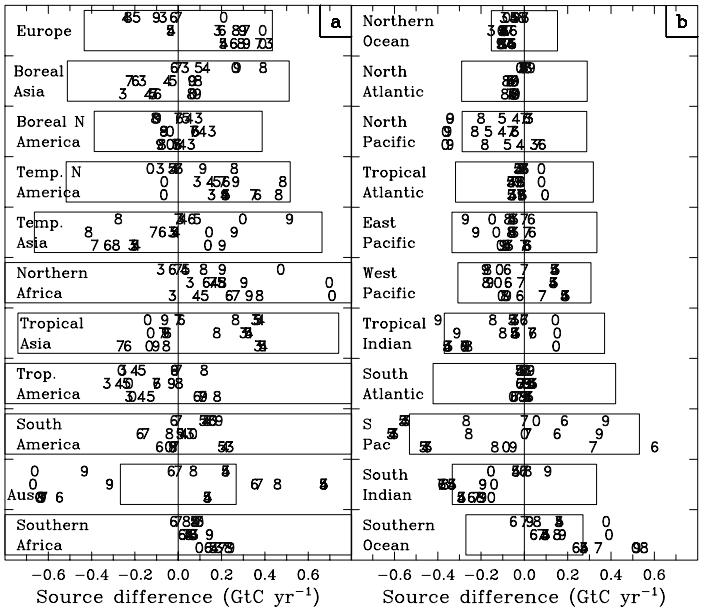


*Fig. 2.* Difference in mean estimated source between the control inversion and inversions with different networks as indicated by the numbers for (a) land and (b) ocean regions. The regions are arranged approximately in their north–south order. The bottom row in each box is NOAA networks, the middle row is NOAA+CSIRO networks and the top row is ALL networks. The number indicates the record-completeness criterion: 100% (0), 90% (9), 80% (8), 70% (7), 60% (6), 50% (5), 40% (4), 30% (3). The control inversion is the ALL case with 70% criterion so the '7' in the top row always lies on the zero difference line. The box shows the magnitude of the within-model source uncertainty estimated in the control case. The off-scale magnitudes for the Northern African, Tropical American and Southern African uncertainties are 0.97, 1.06 and 0.93 Gt C $yr^{-1}$, respectively.

contrary to the observed concentration difference between these records. Hence, the inversion is unable to fit the data. If the (NOAA-only, 50%) inversion is run without including the Takahashi fluxes, there is little change ($-0.08$ Gt C $yr^{-1}$) to the South Pacific source estimate, but the data mismatches are smaller at all but one of the 10 sites between 10–60°S. This suggests that the Takahashi air–sea flux distribution within the South Pacific region is not compatible with the atmospheric concentration data.

All but one estimate for the Southern Ocean region is more positive than the control estimate ($-0.5$ Gt C $yr^{-1}$). This is noteworthy since the control case gave a significantly smaller sink than the prior estimate based on ocean data ($-0.9$ Gt C $yr^{-1}$). This finding suggests that for most networks, the discrepancy with ocean measurements is larger rather than smaller than that indicated by the control. Gurney et al. (2002) discuss a possible reconciliation between atmospheric and oceanic derived flux estimates for this region, based on recent ocean measurements for winter that are not included in the Takahashi air–sea flux estimates.

*3.1.1. Australian case.* Australian mean source estimates and uncertainties are shown in Fig. 3. The results for the smallest (100%) networks are all similar with relatively large within-model uncertainties (i.e. little reduction from the prior uncertainty) and small between-model uncertainties. This uncertainty behaviour is expected when there are few data to constrain the source estimate. In the 90% cases, additional sites in the NOAA+CSIRO and the ALL cases increase the mean source, decrease the within-model uncertainty and increase the between-model uncertainty. Cape Ferguson (19°S, 147°E) is largely responsible in the NOAA+CSIRO case, while Amsterdam Island (38°S, 78°E) also influences the ALL case.

The sensitivity of the source estimate to Cape Ferguson is linked with the inability of the inversion to fit the input observations. In the NOAA case, the Cape Grim (41°S, 145°E) mean data mismatch was 0.13 ppm averaged over the 16 models. In the

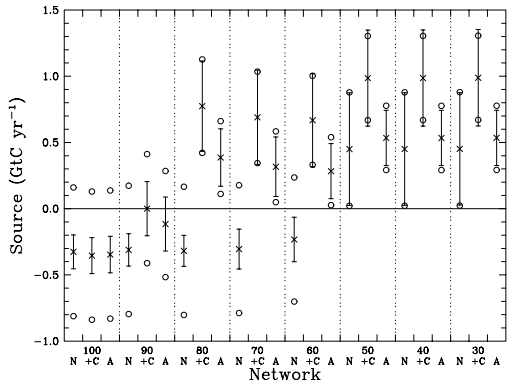


*Fig. 3.* Australian region source estimates for different networks, indicated by the record-completeness criterion (100–30%) (left to right) and the measuring programs included: NOAA only (N), NOAA+CSIRO (+C), ALL (A). The mean source across models is indicated by the × and the standard deviation across models (the between-model uncertainty) by the error bar. The circles indicate the mean within-model source uncertainty returned by the inversion.

NOAA+CSIRO case the mismatch is increased to 0.25 ppm (by the increased source), while the mismatch for Cape Ferguson is −0.15 ppm. The data suggest that the assumed spatial pattern of sources in Australia is incorrect with larger sources required in the northern part of the continent relative to the south. Alternatively there could be an error in transport, but this is less likely since the sign of the data mismatch is the same for all transport models.

The increased estimate in the NOAA+CSIRO 80% case is due to the inclusion of Darwin (12°S, 131°E), which has a concentration about 3 ppm higher than Cape Ferguson. Despite increasing the source, the inversion fails to fit the data; the mean data mismatch is −2.48 ppm. The data at Darwin are often collected under light wind conditions and are consequently subject to local sources (R. Francey, personal communication, 2001). The inversion is not designed to incorporate this local signal and Darwin should be excluded from inversions using large regions. The 80% ALL case includes Baring Head (41°S, 175°E) and this site results in a reduced source estimate and a 22% decrease in within-model uncertainty relative to the 80% NOAA+CSIRO case. The reduction occurs because Baring Head receives a strong signal from New Zealand and, since the inversion includes New Zealand as part of the Australian region, the uncertainty on the whole region decreases.

One more change in the estimated sources deserves comment. The 50% NOAA case gives a source that is almost 0.6 Gt C yr$^{-1}$ larger than the 60% case and between-model uncertainty increases by about 250%. The Australian flux appears to be partially compensating the South Pacific region, which shows a decrease in source of about 1 Gt C yr$^{-1}$, due to the inclusion of Easter Island data. The magnitude of the compensating Australian increase is influenced by the 35°S Pacific ship data and particularly the strength of a model's response at this location relative to the response at Cape Grim due to Australian sources. The seven models with a larger response at Cape Grim gave smaller increases in the Australian source (0.42 Gt C yr$^{-1}$ on average) than the nine models with a larger response at the 35°S ship location (0.89 Gt C yr$^{-1}$ average source increase). This different sensitivity to the inclusion of the 35°S ship data results in the increased between-model uncertainty.

*3.1.2. Individual model sensitivity.* We consider now whether all models give similar or variable changes in sources with changing data networks. Figure 4 shows a measure of this variability. We only use the ALL cases and calculate the change in source as the network increases for each model, e.g. we take the difference of the source estimated with the 100%

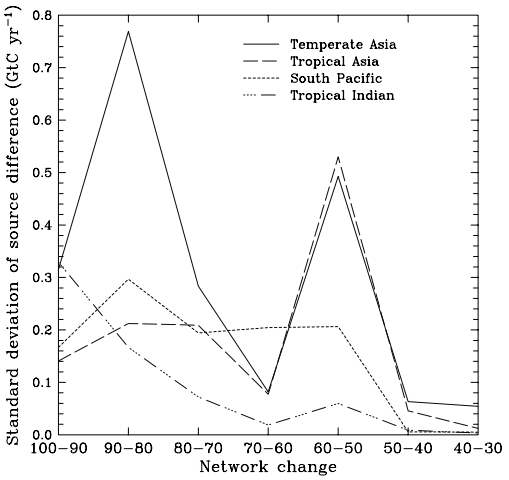


*Fig. 4.* Standard deviation, across models, of the difference in source between inversions with different networks. Only the ALL cases are shown and the source differences are taken between a given network and the next largest in size, e.g. 100–90 indicates the difference between the 100% ALL network and the 90% ALL network. Four regions that give larger standard deviations are shown. The line identification is given in the key.

network and the 90% network for each model. We then calculate the standard deviations of these 16 source differences (for each region and each change in network). The regions are shown by separate lines in Fig. 4, while the change in network is represented in the $x$ direction. A low standard deviation indicates that all models give similar changes in source as the network increases while high standard deviations indicate that the source changes are more variable.

We present four regions in Fig. 4, the two land and two ocean regions that give the largest standard deviations. In general, the standard deviations are larger for land than ocean regions. There is also a general tendency to smaller standard deviations as the number of sites in the network increases. Large standard deviations tend to occur when there are larger mean source differences and vice versa. Thus the standard deviations are low for the 50–40% and 40–30% source differences because the sources themselves change little for these larger networks, to which relatively few new sites are being added.

The largest standard deviation is for the 90–80% case for temperate Asia. We examine this region in more detail shortly. Tropical Asia produces the second largest standard deviation, in the 60–50% case. This is associated with different model responses to the addition of South China Sea (SCS) ship data. While most models give large positive source changes (up to 1.2 Gt C $yr^{-1}$) when the SCS data are added, three models give almost no change and one model gives a large negative change ($-0.6$ Gt C $yr^{-1}$). The largest ocean standard deviation is for the tropical Indian region, 100–90% case, and is associated with the addition of the Seychelles (5°S, 55°E) record. The South Pacific gives more consistently large standard deviations that, as discussed above, are associated with different model responses to the addition of Pacific ocean ship and Easter Island data.

Figure 5 shows the temperate Asian sources and within-model uncertainties for the eight ALL networks. There are two network transitions (90 to 80% and 60 to 50%) where the reductions in within-model uncertainty are larger and the source estimates change substantially and variably across models. These transitions correspond to the addition of Ulaan Uul in the 80% network and Mt. Waliguan in the 50% network. The within-model uncertainties are quite variable across models and are determined by the concentration responses at these sites from the temperate Asian region source. For example, the TM3 response at Ulaan Uul is 3.3 ppm, while other models range

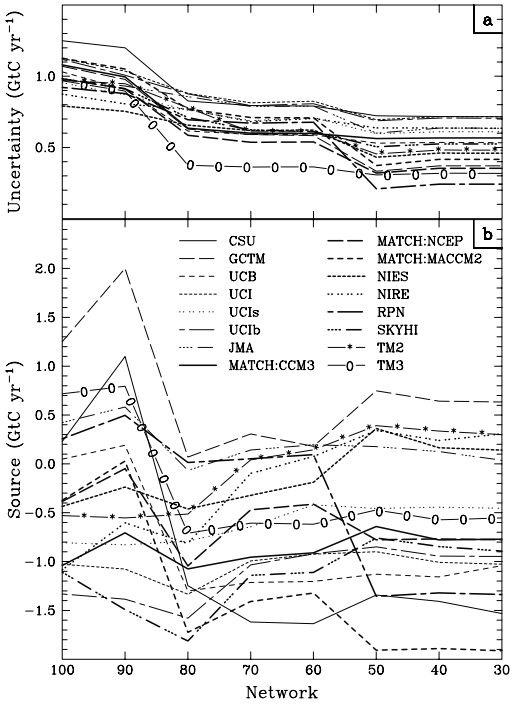


*Fig. 5.* Source uncertainties (a) and estimates (b) for each model for temperate Asia for each of the ALL networks. The line identification is given in the key.

from 2.2 to 2.9 ppm. Consequently the TM3 uncertainty is substantially lower (0.38 Gt C $yr^{-1}$) than the other models (0.59–0.88 Gt C $yr^{-1}$).

Most models give a decrease in source with the addition of the Ulaan Uul site (80% network), but the magnitude of the source change varies greatly from $-2.3$ to 0.0 Gt C $yr^{-1}$ . The source change is greater than the uncertainty for a third of the models. The range of source estimates is smaller in the 80% network case (1.9 Gt C $yr^{-1}$) compared to the 90% case (3.5 Gt C $yr^{-1}$), presumably due to the strong constraint provided by adding a site within the region being estimated. By contrast, the addition of Mt. Waliguan as part of the 50% network, increases the source range across models to 2.7 Gt C $yr^{-1}$ since the models respond differently to the inclusion of this site. This variable sensitivity to the addition of Mt. Waliguan data is in part due to the 'rectifier' contribution from the covariance of the seasonal cycles of biospheric fluxes and atmospheric transport. If the inversion is run without the neutral biosphere response (as in section 3.2 of Gurney et al., 2003) then the range of source

estimates is reduced, particularly in the 50% case, when an increased range is no longer produced by the Mt. Waliguan data. Clearly, the magnitude and spatial distribution of the rectifier is an important component of the model–model differences. It will be important to check whether similar model differences are also seen in inversions from monthly mean data, when the rectifier does not have to be included as a separate response.

### 3.2. *Time period of data*

Figure 6 summarises the inversion sensitivity to different years of data. For each region, the leftmost value in each box is the control run, followed by the 1995–1997, 1992–1994 and 1989–1991 data periods, respectively. For most regions, using different years for the inversion does not result in significant deviations from the control; the mean sources lie within the mean uncertainty of the control run. Only temperate North America for 1989–1991 and the tropical Indian Ocean for 1995–1997 and 1989–1991 exceed a 0.5 Gt C $yr^{-1}$ difference from the control. We discuss these two regions in more detail shortly. Since the control case encompasses all but 1997 in the 1992–1994 and 1995–1997 cases, the sources for these two time periods show deviations of opposite sign from the control case for almost all regions.

In order to determine what contribution the change in the global growth rate and the fossil fuel response

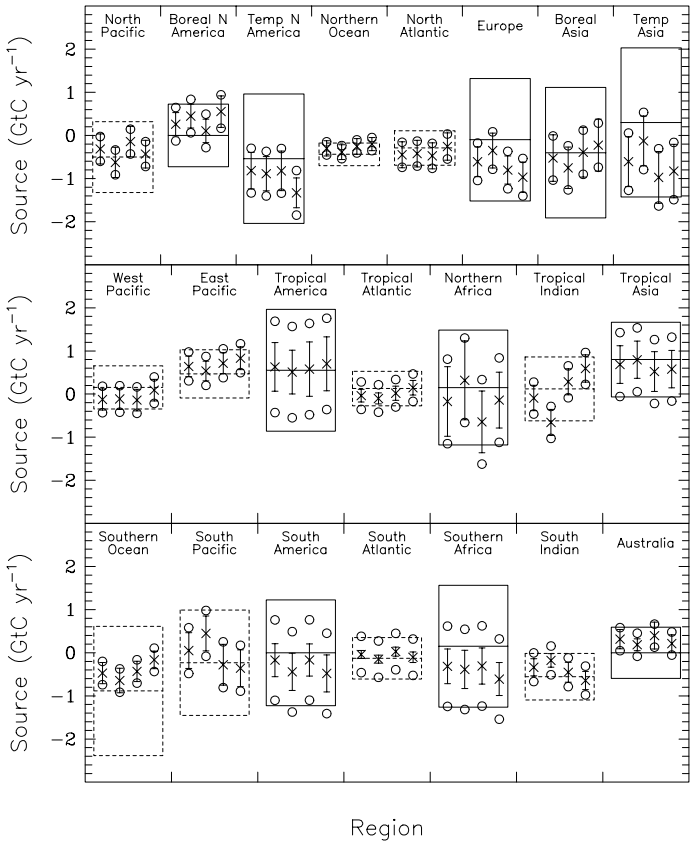


*Fig. 6.* Model mean inversion results for all 22 basis regions using data from different time periods. The leftmost value in each box is the control case 1992–1996, followed by 1995–1997, 1992–1994 and 1989–1991, respectively. Mean source estimates (including the background ocean fluxes) are indicated by the ×, mean within-model uncertainty by the ○ and between-model uncertainty (the standard deviation across model source estimates) by the bar. For each land (solid line) and ocean (dashed line) region, the boxes represent the prior source estimate (central horizontal line) and prior uncertainty. Regions are arranged to approximate their north–south and east–west relationship.

makes to the differences in source estimates, we have performed a sensitivity test in which these two parameters are retained at their control values. Results indicate that source differences due to changes in the global growth rate constraint are generally spread over all regions, rather than influencing a particular region. Use of different fossil responses also does not have a large influence, as the distribution and magnitude of 1990 and 1995 fossil-fuel emissions are mostly similar. Only one test causes a regional change greater than 0.2 Gt C $yr^{-1}$ (1989–1991 temperate Eurasia increases by 0.29 Gt C $yr^{-1}$ when the control fossil-fuel mixture is used). Thus the differences in the inversion results are mostly caused by interannual differences in the GLOBALVIEW-$CO_2$ dataset.

The variation in tropical Indian ocean source with time period is determined by the data at Seychelles and, to a lesser extent, Darwin. Running the inversions without these two sites collapses the 1995–1997, 1992–1994 and 1989–1991 mean source differences from the control from −0.56, 0.37 and 0.69 Gt C $yr^{-1}$ to 0.05, −0.05 and 0.07 Gt C $yr^{-1}$, respectively. The temporal variation is very similar for all the individual models for this region, principally because there are so few sites nearby. This strong dependence on the Seychelles data will be problematic if its interannual variability is not representative of the whole tropical Indian ocean. The behaviour of temperate North America is rather different. The response of individual models is more variable, and the −0.51 Gt C $yr^{-1}$ source difference in the 1989–1991 case does not appear to be dependent on any one or two individual sites. Several sensitivity tests removing multiple sites failed to significantly reduce the difference. The implication is that the data for sites in and around this region have consistent interannual variations. Thus we might expect to place more confidence in the temperate North American source variations than the tropical Indian ocean ones.

### *3.3. Data selection*

Three sets of inversions have been run to compare cases with more ('flask-like') and less ('nearest-grid') data selection with a new control case. The inversion configuration for the three cases is different, in two ways, to the control case used above. Firstly, two models were excluded from these inversions. The CSU model was not used due to the numerical properties of the advection scheme that this model employs; simulated timeseries do not show a clear baseline signal, and so the method used here for data selection cannot be successfully applied to this model. The SKYHI model was not used because high-frequency time series were not submitted for this model so data selection could not be performed. Secondly, we have removed the Pacific ocean ship data from these inversions, as high-frequency timeseries were not part of the submitted model output so baseline selection cannot be applied.

Figure 7 shows the mean results from the three inversions. Overall the results for the new control are very similar to those from the previous control. The largest differences in source (up to 0.25 Gt C $yr^{-1}$) are around the Pacific region and are associated with the removal of the Pacific ship data. Comparing the nearest-grid case with the new control case, five regions show a change in mean source greater than 0.3 Gt C $yr^{-1}$: temperate North America, temperate Asia, tropical America, tropical Asia and northern Africa. In these model-mean results, none of the changes moves the mean source outside of the range of sources given by the control case uncertainty. However, there are much larger changes in some individual models as seen by the increased between-model uncertainties for many regions. For example, for temperate North America, the nearest-grid case gives a larger sink than the control by over 1.0 Gt C $yr^{-1}$ for three models with the maximum difference being −2.8 Gt C $yr^{-1}$ . The Key Biscayne site is responsible for these large changes. If the inversion is run without this site then the mean model source difference is 0.08 Gt C $yr^{-1}$ instead of −0.43 Gt C $yr^{-1}$, and the range across individual models is −0.26 to 0.37 Gt C $yr^{-1}$.

The removal of Key Biscayne also reduces the mean source differences for tropical America and northern Africa, indicating that the changes in these regions were mostly a compensation for the change in temperate North America. It is worth commenting on the sign of the differences found; when Key Biscayne is moved onto or towards the land, the temperate North American sink tends to get larger. This occurs because the inversion effectively uses fixed fossil, neutral biosphere and ocean responses from which to invert. Shifting Key Biscayne towards land significantly increases the fossil contribution at this site, particularly in some models, and so the inversion finds a larger sink to compensate for this extra fossil response. Similar reasoning can explain the change in the temperate Asian source, but in this case the Tae-ahn site is the dominant contributor to the change and tropical Asia

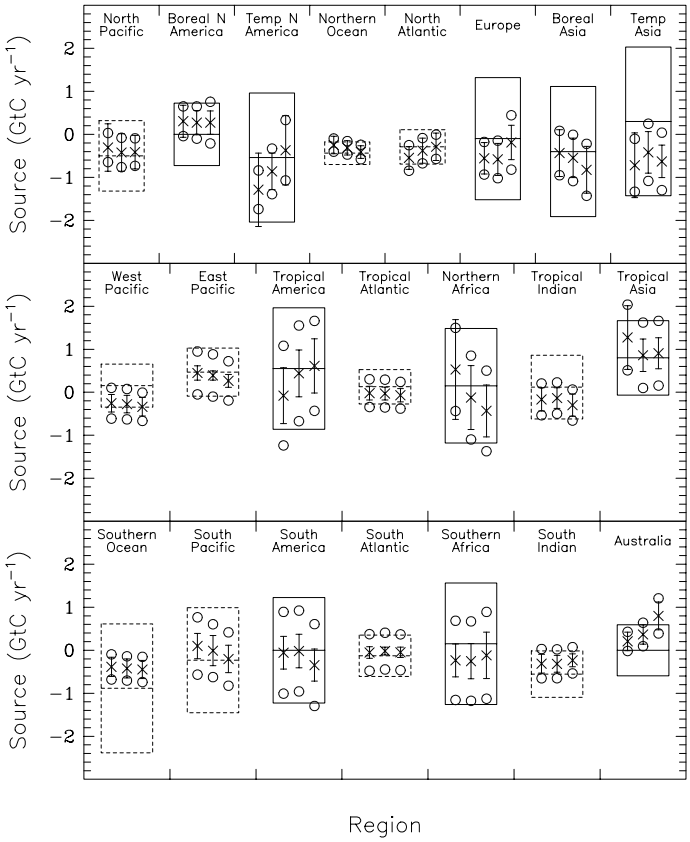


*Fig. 7.* As Fig. 6 but showing mean sources and uncertainties for three sets of inversions with different data selection strategies. Left is the 'nearest-grid' inversion, centre is the modified control inversion, right is the 'flask-like' inversion.

and northern Africa are the regions that compensate changes in temperate Asia.

Comparing the flask-like selection with the control case, there are five land regions with source differences greater than 0.3 Gt C $yr^{-1}$: temperate North America, Europe, Australia (positive differences) and northern Africa and South America (negative differences). It seems likely that the regions with the positive differences are directly influenced by the change in site responses due to selection, while those regions with negative differences are probably compensating the positive changes. The two regions with largest positive changes, temperate North America (0.49 Gt C $yr^{-1}$) and Australia (0.43 Gt C $yr^{-1}$), are quite different in the consistency of the changes across models. Temperate North America shows more variable changes, from −0.3 to 0.9 Gt C $yr^{-1}$ with one outlier at 2.4 Gt C $yr^{-1}$ , whereas the Australian changes range from 0.2 to 0.6 Gt C $yr^{-1}$ . However, the greater consistency for Australia is due to the relatively small (0.59 Gt C $yr^{-1}$) prior uncertainty for that region. If this uncertainty is increased to 1.5 Gt C $yr^{-1}$, the magnitude used for temperate North America, then the mean change in source due to selection increases to 1.0 Gt C $yr^{-1}$ , with a range across models of 0.2–2.2 Gt C $yr^{-1}$.

The estimated uncertainties change very little for the inversions with more or less selection. Uncertainty changes for land regions tend to be slightly larger than for ocean regions. In the less-selection case, within-model uncertainties decrease for land regions and increase for ocean regions, while in the more-selection case the land uncertainties increase and the ocean ones decrease. This is expected, as selection is intended to remove the signal from land regions and thus uncertainty should increase as more selection is performed. The changes in between-model uncertainty are also larger for land than ocean regions but the change is positive, i.e. to larger between-model

uncertainty, for both more-selection and less-selection cases. It is possible that in the less-selection, nearest-grid case, the movement of sites onto land increases model differences caused by how the spatial distribution of sources is represented on the different grids of each model. Transport differences may also be accentuated over land. In the more-selection case, the attempt to weaken the local response will allow more distant sites to influence the source estimates for a given region. Any differences in model transport to those sites may be seen as an increased between-model uncertainty.

### 3.4. *Data uncertainty*

Figure 8 shows the estimated sources and uncertainties for the inversions in which the data uncertainties were changed. The first and second cases from the left in each box are those in which the data uncertainties were halved and doubled. We find that as data uncertainty is decreased, the within-model uncertainty decreases and between-model uncertainty increases and vice versa. A decrease in data uncertainty forces the inversion to fit the data more closely. This accentuates model transport differences and hence larger between-model uncertainty results. The control case, which used data uncertainties scaled such that the inversion gave $\chi^2 \approx 1$, typically gives within-model uncertainties that are similar or slightly larger in magnitude that the between-model uncertainties. This would seem to be a desirable choice. It suggests that most of the time an individual model will give a source that is within the range of sources determined by the mean source and uncertainty across models. Halving and doubling the

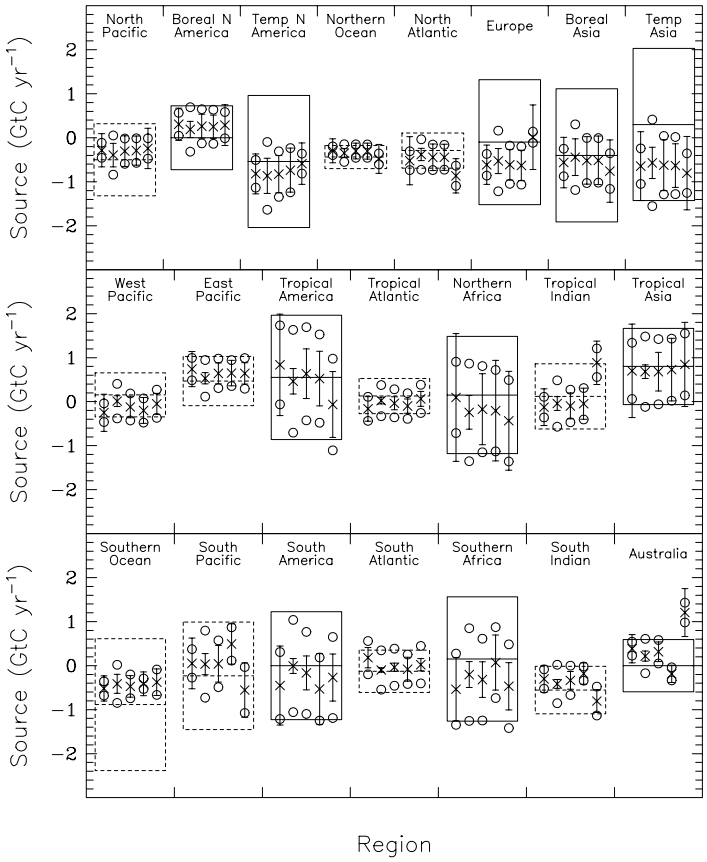


*Fig. 8.* As Fig. 6 but showing mean sources and uncertainties for five sets of inversions with different data uncertainties. The control data uncertainties were multiplied by 0.5 (far left) and 2.0 (left). The control inversion results are in the centre of each box. Also shown are inversions with no minimum data uncertainty (right) and constant 0.3 ppm data uncertainty (far right).

data uncertainty also produces changes in the mean estimated sources, but these changes are generally small relative to the uncertainty range of the control case.

We now consider the cases where the data uncertainties were distributed differently. The fourth case from the left allowed data uncertainties less than the 0.25 ppm minimum used in the control. There is little change from the control inversion results except in the southern regions. This is anticipated, since it is mostly sites in the southern mid-high latitudes that are affected by the minimum criteria. For these southern regions the within-model uncertainty tends to decrease and the between-model uncertainty tends to increase. This follows the general pattern when data uncertainty is reduced. The mean source estimates change by more than 0.1 Gt C $yr^{-1}$ for all the southern regions except the South Atlantic and the Southern Ocean. The changes in source are not driven by just one or two sites. It appears that the inversion is attempting to fit longitudinal concentration variations between sites within the Southern Ocean region and around the Antarctic coast. Since the Southern Ocean is treated as one large region, the improved data fit can only be accommodated by adjusting sources in the neighbouring regions to the north even though this is unlikely to be the real cause of the longitudinal variations in concentration. Rather, the longitudinal variations imply that the spatial distribution prescribed for the Southern Ocean region should be adjusted. This example illustrates the potential for biased source estimates due to spatial aggregation if the data uncertainties being used are too small.

The fifth case from the left uses constant data uncertainties of 0.3 ppm at all sites. This is a smaller data uncertainty than the control for about two thirds of the sites. Consequently, in general, the results show reduced within-model source uncertainties relative to the control and increased between-model uncertainties. Europe is an extreme example. Europe is also one of the regions that shows a substantial change in mean estimated source. In the northern regions there is a shift in uptake from land to ocean. In the tropics, the Indian Ocean changes from a small sink to a moderate source. This region appears to be quite sensitive to the data uncertainty applied to Cape Rama. In the southern regions, Australia shows the largest change in estimated source. This results from placing a low data uncertainty on the Darwin mean concentration, which is anomalously high. Thus, the Australian source is increased to try and better fit the Darwin data. The increased sink in the South Pacific acts to compensate for the change in Australia.

## 4. Discussion and conclusions

Much detailed information has been presented from the various sensitivity tests. Here we attempt to highlight the main findings particularly where these might provide guidance for how annual mean inversions are best set up. Overall, we have seen that for most of the sensitivity tests, the mean estimated sources lie within the range of sources determined by the within-model uncertainty from the control inversion. This would indicate that the mean sources and their uncertainties estimated from the control inversion are reasonably robust for most regions. It also suggests that the data-related choices made in the inversion set-up for the control case were reasonable.

Data network choices remain one of the more difficult decisions when setting up an inversion. For annual mean inversions, such as used here, it is easy to perform many tests. The difficulty is in interpreting the sensitivity obtained. For example, a large sensitivity in a data sparse region may be quite appropriate as new, valid information is being added to the inversion. By contrast, a similar sensitivity in a region where there are many sites suggests a problem with the new measurement or with the assumed spatial distribution of sources within regions. One indicator that a site should be examined more closely is the ability of the inversion to fit the data at that location. For example, if the data mismatch is more than twice the data uncertainty applied at that site, then a potential problem is implied.

Applying this criterion to the set of network inversions tested here, five sites have data mismatches that are too large in at least some of the cases: Black Sea, Cape Rama, Darwin, Easter Island and Guam. We have already highlighted the sensitivity of the inversion to Darwin and Easter Island. For Darwin, the major problem seemed to be with the representativeness of the measurements. Thus, we would suggest that Darwin data are not well suited to inversion work and should be flagged as such in the GLOBALVIEW dataset. For Easter Island, the problem appears to be more with the spatial distribution of fluxes within the South Pacific region. One solution is to split the South Pacific into more than one region. The other would be to increase the data uncertainties for all sites in the vicinity of the region. This aims to avoid biasing the source estimates due to the incorrect spatial distribution.

Of the other three sites, Black Sea has a short record (only making it into the 30% network) and hence is heavily dependent on the data extension method for determining the mean 1992–1996 concentration. In this continental location, it is probably unrealistic to be this reliant on data extension and the choice of a 70%-complete criterion for the control inversion seems to be reasonable. Both Cape Rama and Guam give reduced data mismatches when the inversion is run without the seasonal rectifier contribution. Cape Rama shows a low, positive correlation (0.22) and Guam, a higher correlation (0.75) between the data mismatch for individual models and the magnitude of the seasonal biospheric response for each model. Again this suggests a spatial distribution error, though it is not clear whether it is with the underlying biospheric sources or in the pattern of rectification produced by the transport models. Larger data uncertainties may be required to allow for this.

There has been little work until now on the choice of data uncertainties for annual mean inversions. The sensitivity that we have found suggests that data uncertainty choices are more important than had previously been assumed. Clearly spatially variable uncertainties are preferable to constant ones to accommodate the different locations of data records and our ability to model those locations. Scaling the magnitudes of the data uncertainties to give $\chi^2 \approx 1$ seems to give a good balance between within-model and between-model uncertainty. Data uncertainties need to be large enough to absorb errors in source spatial distribution within regions. A large between-model uncertainty in a given region may act as an indicator that the inversion is 'over-fitting' the data in that region and that a larger data uncertainty is appropriate.

Perhaps surprisingly, data selection has a relatively small impact in these annual mean inversions, at least in the mean across models. The practice of moving sampling locations offshore for coastal sites provides a good, easy method for taking some account of selection issues. The small impact seen here may not extend to inversions that solve for the seasonal cycle. This will need to be considered in the future.

Similarly to the small impact found for data selection, we have found that the mean inversion results are relatively insensitive to using different data time periods. While interannual variations in sources are suggested in some regions, the variations are almost always less than the estimated source uncertainties. The inversions presented here are designed to estimate long-term mean fluxes since we use equilibrium response functions. As such, it is preferable to use as long a data period as possible given the constraints of data gaps and changing networks. One of the next stages of the TransCom 3 project will be to perform inversions using monthly time series data to give interannual varying sources. It will be interesting to compare the sources obtained here for the different 3-yr periods with those that will be obtained from the full interannual inversion.

We have found that there are clear advantages in being able to perform sensitivity tests over a range of transport models. Where the sensitivity is consistent across models, we can have more confidence in our conclusions. We are also able to ascertain when individual models give sensitivities that are large and unrepresentative and would have misled if we were reliant only on that model. For this reason, the TransCom 3 dataset may have an ongoing role in providing a set of model responses that can be used to test inversion methodology choices. It is much easier to run multiple sensitivity tests with annual mean inversions than with interannual ones. Thus, the knowledge of sensitivities gained here can provide useful input to decisions about inversion set-up for other inversions such as the TransCom 3 interannual cases.

## 5. Acknowledgements

We thank Dr Ying-Ping Wang for helpful comments on this manuscript. TransCom 3 was made possible through support from the National Science Foundation (OCE-9900310), the National Oceanic and Atmospheric Administration (NA67RJ0152, Amend 30) and the International Geosphere Biosphere Program/Global Analysis, Interpretation and Modeling Project.

## REFERENCES

Baker, D. F. 2001. *Sources and sinks of atmospheric $CO_2$ estimated from batch least-squares inversions of $CO_2$ concentration measurements*. Ph.D. Thesis, Princeton University, U.S.A.

Bousquet, P., Ciais, P., Peylin, P., Ramonet, M. and Monfray, P. 1999a. Inverse modeling of annual atmospheric $CO_2$ sources and sinks 1. Method and control inversion. *J. Geophys. Res.* **104**, 26 161–26 178.

Bousquet, P., Peylin, P., Ciais, P., Ramonet, M. and Monfray, P. 1999b. Inverse modeling of annual atmospheric $CO_2$ sources and sinks 2. Sensitivity study. *J. Geophys. Res.* **104**, 26 179–26 193.

Bousquet, P. 1997. *Inversion of net $CO_2$ fluxes: Assimilation of atmospheric measurements of $CO_2$ and $^{13}CO_2$ in a three-dimensional transport model* (in French). Ph.D. Thesis, L'Univ. Paris VI, France.

Fan, S., Gloor, M., Mahlman, J., Pacala, S., Sarmiento, J., Takahashi, T. and Tans, P. 1998. A large terrestrial carbon sink in North America implied by atmospheric and oceanic $CO_2$ data and models. *Science* **282**, 442–446.

Francey, R. J., Tans, P. P., Allison, C. E., Enting, I. G., White, J. W. C. and Trolier, M. 1995. Changes in oceanic and terrestrial carbon uptake since 1982. *Nature* **373**, 326–330.

GLOBALVIEW-$CO_2$. Cooperative Atmospheric Data Integration Project–Carbon Dioxide. CD-ROM, NOAA CMDL, Boulder, Colorado 2000. [Also available on Internet via anonymous FTP to ftp.cmdl.noaa.gov, Path: ccg/co2/GLOBALVIEW].

GLOBALVIEW-$CO_2$. Cooperative Atmospheric Data Integration Project–Carbon Dioxide. CD-ROM, NOAA CMDL, Boulder, Colorado 2001. [Also available on Internet via anonymous FTP to ftp.cmdl.noaa.gov, Path: ccg/co2/GLOBALVIEW].

Gurney, K., Law, R., Rayner, P. and Denning, A. S. 2000. TransCom 3 Experimental Protocol [Electronic publication]. Atmospheric science paper no. 707, Department of Atmospheric Science, Colorado State University, Fort Collins, USA. (http://transcom.colostate.edu/TransCom_3/T3_Protocol_and_Registration/body_t3_protocol_and_registration.html).

Gurney, K. R., Law, R. M., Denning, A. S., Rayner, P. J., Baker, D., Bousquet, P., Bruhwiler, L., Chen, Y. H., Ciais, P., Fan, S., Fung, I. Y., Gloor, M., Heimann, M., Higuchi, K., John, J., Maki, T., Maksyutov, S., Masarie, K., Peylin, P., Prather, M., Pak, B. C., Randerson, J., Sarmiento, J., Taguchi, S., Takahashi, T. and Yuen, C. W. 2002. Towards robust regional estimates of $CO_2$ sources and sinks using atmospheric transport models. *Nature* **415**, 626–630.

Gurney, K. R., Law, R. M., Denning, A. S., Rayner, P. J., Baker, D., Bousquet, P., Bruhwiler, L., Chen, Y. H., Ciais, P., Fan, S., Fung, I. Y., Gloor, M., Heimann, M., Higuchi, K., John, J., Kowalczyk, E., Maki, T., Maksyutov, S., Peylin, P., Prather, M., Pak, B. C., Sarmiento, J., Taguchi, S., Takahashi, T. and Yuen, C. W. 2003. TransCom 3 $CO_2$ inversion intercomparison: 1. Annual mean control results and sensitivity to transport and prior flux information. *Tellus* **55B**, this issue.

Kaminski, T., Rayner, P. J., Heimann, M. and Enting, I.G. 2001. On aggregation errors in atmospheric transport inversions. *J. Geophys. Res.* **106**, 4703–4715.

Keeling, C. D., Whorf, T. P., Wahlen, M. and van der Plicht, J. 1995. Interannual extremes in the rate of rise of atmospheric carbon dioxide since 1980. *Nature* **375**, 666–670.

Law, R. 1996. The selection of model-generated $CO_2$ data: a case study with seasonal biospheric sources. *Tellus* **48B**, 474–486.

Masarie, K. A., and Tans, P. P. 1995. Extension and integration of atmospheric carbon dioxide data into a globally consistent measurement record. *J. Geophys. Res.* **100**, 11 593–11 610.

Masarie, K. A., Langenfelds, R. L., Allison, C. E., Conway, T. J., Dlugokencky, E. J., Francey, R. J., Novelli, P. C., Steele, L. P., Tans, P. P., Vaughn, B. and White, J. W. C. 2001. NOAA/CSIRO Flask air intercomparison experiment: A strategy for directly assessing consistency among atmospheric measurements made by independent laboratories. *J. Geophys. Res.* **106**, 20 445–20 464.

Pacala, S. W., Hurtt, G. C., Baker, D., Peylin, P., Houghton, R. A., Birdsey, R. A., Heath, L., Sundquist, E. T., Stallard, R. F., Ciais, P., Moorcroft, P., Caspersen, J. P., Shevliakova, E., Moore, B., Kohlmaier, G., Holland, E., Gloor, M., Harmon, M. E., Fan, S. M., Sarmiento, J. L., Goodale, C. L., Schimel, D. and Field, C. B. 2001. Consistent land- and atmosphere-based U.S. carbon sink estimates. *Science* **292**, 2316–2320.

Ramonet, M. and Monfray, P. 1996. $CO_2$ baseline concept in 3-D atmospheric transport models. *Tellus* **48B**, 502–520.

Rayner, P. J., Enting, I. G., Francey, R. J. and Langenfelds, R. L. 1999. Reconstructing the recent carbon cycle from atmospheric $CO_2$, $\delta^{13}C$ and $O_2/N_2$ observations. *Tellus* **51B**, 213–232.

Takahashi, T., Wanninkhof, R. H., Feely, R. A., Weiss, R. F., Chipman, D. W., Bates, N., Olafsson, J., Sabine, C. and Sutherland, S. C. 1999. Net sea–air $CO_2$ flux over the global oceans: An improved estimate based on the sea-air $pCO_2$ difference. *Extended abstracts of the 2nd International $CO_2$ in the Oceans Symposium, Tsukuba, Japan, January 18–22, 1999,* 18-01.